Biosensors and Bioelectronics 164 (2020) 112324

Contents lists available at ScienceDirect

Biosensors and Bioelectronics

journal homepage: http://www.elsevier.com/locate/bios

# Carboxyl functionalized gold nanorods for sensitive visual detection of biomolecules

Friedrich Scholz [a,*], Lukas Rüttinger [a], Theresa Heckmann [a], Lisa Freund [a], Anne-Marie Gad [a], Tobias Fischer [b], Andreas Gütter [a], Hans Hermann Söffing [a]

[a] Senova Gesellschaft für Biowissenschaft und Technik mbH, Industriestraße 8, 99427, Weimar, Germany
[b] fzmb GmbH Research Centre of Medical Technology and Biotechnology, Geranienweg 7, 99947, Bad Langensalza, Germany

ARTICLE INFO

*Keywords:*
Lateral flow immunoassay
Coloured nanoparticles
Gold nanorods
Surface modification

ABSTRACT

Antibody-modified gold nanomaterials are central to many novel biosensing technologies for example the lateral flow assays technology. The combination of the specificity, provided by antibody–antigen interactions, and the unique optical properties of nanomaterials provide excellent properties for biosensors. Here, we present the use of gold nanorods (GNR) with the localized Surface Plasmon Resonance (LSPR) peak in the visible range for biomarker detection. The colour of the GNR can be tuned by the reaction conditions to provide multi-coloured gold nanorod conjugates. These antibody functionalized GNR have the potential to provide significant improvements in multiplexed analysis and sensitivity compared to conventional gold nanoparticle based lateral flow assays. However, a major challenge is the synthesis of stable conjugates that resist aggregation in samples with high ionic strength, (e.g. salt solutions) and allow highly sensitive detection of proteins. A detailed investigation of different reagents for the functionalization of gold nanorod materials are reported. An antibody modified GNR based lateral flow assay is validated for the determination of C-reactive Protein (CRP).

## 1. Introduction

Lateral flow assay (LFA) biosensors are simple devices intended to detect the presence of a target analyte in a given sample. The benefits of LFA biosensors include short times to obtain test results, a user-friendly test setup, low cost, and long-term stability (Posthuma-Trumpie et al., 2009; Dzantiev et al., 2014). Consequently, LFA has recently seen wide spread applications in the fields of medical diagnosis, animal health, agriculture and environmental analysis (Posthuma-Trumpie et al., 2009; Kavosi et al., 2014; Sajid et al., 2015; Huang et al., 2016).

In a typical testing procedure, the mobile phase is first pulled through the stationary phase by capillary forces. Afterwards the mobile phase passes through a capture zone, where trapped labels, e.g., antibody-conjugated nanoparticles, accumulate in concentration until they are visually detectable. Indeed, such a test does not require any sample preparation or electronic devices, and only relies on visual detection (Huang et al., 2016).

Most often commercial colorimetric LFA use spherical gold nanoparticles (GNP) as labels, with diameter comprises between 20 and 60 nm (Koczula and Gallotta, 2016). These nanoparticles exhibit a surface plasmon resonance (SPR) absorption maxima around 525 nm, causing red coloured particles and allow read out of the LFA with the naked eye. GNP are easy to conjugate with proteins and can be produced in large scale and cost saving (Posthuma-Trumpie et al., 2009; Kavosi et al., 2014; Huang et al., 2016). Those advantages in combination with the high extinction coefficient at 525 nm, due to the SPR, make GNP very suitable for LFA applications (Liu et al., 2007). Most organic molecules and biomolecules have much lower extinction coefficient than gold nanoparticles and therefore they are less suited as labels for LFA (Liu et al., 2007). Recently, great efforts have been made to improve the sensitivity of the GNP-based LFAs by different approaches. Fluorescent- or enzyme-based LFA were reported to improve sensitivity (Parolo et al., 2013; Xie et al., 2014; Shin and Park, 2016).

The use of gold nanomaterials in surface-enhanced raman spectroscopy (SERS) based LFA is a very current research area (Fu et al., 2016; Lee et al., 2017). Among other things, GNR are used as labels, whereby the absorption maxima are mostly in the IR range (>690 nm) (Lin et al., 2019; Lu et al., 2020). However, using other labels than coloured particles increase the complexity, the price of the assay or make it necessary to use devices to read out the test strip.

* Corresponding author.
*E-mail address:* f.scholz@senova.de (F. Scholz).

https://doi.org/10.1016/j.bios.2020.112324
Received 6 April 2020; Received in revised form 15 May 2020; Accepted 22 May 2020
Available online 30 May 2020

Two factors can be considered to improve the sensitivity and quantification capability of gold nanomaterial based LFA sensors in the visual detection of target analyts: The use of gold nanomaterials with increased size (Henderson and Stewart, 2002; Aveyard et al., 2007) and the optimization of the functionalization of the gold nanomaterial (Guler and Sarac, 2016).

Size, shape and colour of gold nanoparticles are limited due to the fact, that they will aggregate when grow up to diameters over 100 nm (Laitinen and Vuento, 1996). Therefore, some authors report GNR (Venkataramasubramani and Tang, 2009), other non-spherical nanomaterial (Maiorano et al., 2011; Ji et al., 2015; Zhang et al., 2015; Di Nardo et al., 2017; Anfossi et al., 2019; Di Nardo et al., 2019; Petrakova et al., 2019; Nguyen et al., 2020) and multilayer GNP (Wiriyachaiporn et al., 2015) as label with the aim of improving sensitivity. More specifically, rose like gold nanoparticles or nano popcorns were reported as labels for developing LFAs. These LFA possesses higher optical brightness, better colloidal stability and better sensitivity than using GNP (Di Nardo et al., 2017; Serebrennikova et al., 2018; Anfossi et al., 2019; Zhu et al., 2019). These nanoparticles exhibited a blue colour instead of the red colour of GNP, because the size and shape of GNP have significant influences on the SPR band.

Anyway, all these studies report no data to the size distribution of the nanomaterials. The syntheses are mostly very simple and carried out without controlled growth, which indicates that particles of various sizes are obtained. This is an important fact with regard of the reproducibility of lateral flow assays. Furthermore, the labeling of antibodies is achieved through passive adsorption of proteins on the citrate or carbonate stabilized surfaces of these nanomaterials. Direct adsorption of antibody onto the surface of citrate capped GNPs is the most straightforward approach to forming bioconjugates. The antibodies can interact with negatively charged GNP to form stable conjugates. Protein attachment occurs through a combination of hydrophobic, electrostatic interactions (Meissner et al., 2015) and chemisorption of cysteine through the thiol moiety (Wang et al., 2017).

Moreover, the hydrophobic and electrostatic interactions can alter the antibody structure and attenuate antibody binding activity. Furthermore, it has been argued that noncovalent attachment allows desorption, which can result in short shelf-life and unwanted protein exchange (Puertas et al., 2011).

More robust conjugation strategies have been developed, where the surface of the gold nanomaterial can be modified followed by a covalent bioconjugation (António et al., 2018). Most often carboxyl and thiol cross-linking reagents with different spacers were used for surface modification (Tshikhudo et al., 2004; Liao and Hafner, 2005; Shenoy et al., 2006; Tsai et al., 2010; Gao et al., 2012). The bioconjugation is carried out in a second step through the formation of an amide bond (Guler and Sarac, 2016). Furthermore, the optimization of the crosslinker and the functionalization protocol allows the optimization of the functional properties of the antibody conjugates (Liopo et al., 2012; Wang et al., 2017). Lin also show more stable and more sensitive biosensor by using intelligent linkers for the protein conjugation (Lin et al., 2017). Here the first gold nanorods (GNR) based lateral flow assay on the use of optimized GNR conjugates with different colours is described. GNR as label in an LFA application were first reported by Venkataramasubramani and Tang. They reported the fabrication and characterization of monodispersed GNR of uniform size as well as biofunctionalization of the GNR for biological applications with tunable longitudinal surface plasmon resonance (LSPR) peaks in the infrared range (>700 nm), which cannot be read out with the naked eye (Venkataramasubramani and Tang, 2009).

Since these first description of gold nanorod based LFA the field of plasmonic properties from metallic nanoparticles has become one of the most exciting and active research areas. A lot of syntheses of colloidal GNR with tunable LSPR are reported. But only a few studies reported syntheses with well controlled size and tunable GNR with LSPR less than 700 nm to obtain visible GNR. For example, Wang describes a glass-based biosensor using GNR with LSPR <700 nm (Wang and Tang, 2015).

Tao et al. already describes a SERS based LFA using GNR in the visible range. The GNR obtained show very low sensitivities for the visual LFA application (Tao et al., 2018). This is mainly due to the fact that the functionalization of the GNR has to be adapted specifically for the visual LFA application.

One hurdle in the scalable manufacturing of GNR-based materials is the efficient exchange and removal of cetyltrimethylammonium bromide (CTAB), a micellar surfactant used in the batch synthesis of GNR (Dreaden et al., 2012; Wang and Tang, 2015). CTAB is cationic and moderately cytotoxic and does not allow direct antibody conjugation. CTAB can be removed by multiple washing steps and exchanges with chemisorptive surfactants (e.g., PEGylated thiols or dithiocarbamates). However, CTAB-coated GNR dispersions are frequently destabilized during surfactant exchange, resulting in partial aggregation and low recovery yields. Furthermore, ligand-modified GNR are often contaminated with residual CTAB, which can induce nonspecific protein adsorption (Huff et al., 2007) resulting in decreased specificity.

Inspired by the use of nanomaterials of controlled size and shape and the possibility to optimize the antibody conjugation by using PEGylated thiols or dithiocarbamates, optimized GNR conjugates would be an ideal coloured reagent to enhance the LFA sensitivity and to enable multiplex analyses. Therefore, we use an improved synthesis of GNR with LSPR <700 nm by using additives that also reduces the concentration of CTAB surfactants (Ye et al., 2012). The reduced CTAB concentration allows easy and well controllable functionalization of the GNR with carboxyl and thiol cross-linking reagents. In this work, we systematically investigated the functionalization of GNR and evaluate the stability and the functionality in an LFA application. The preparation of optimized and stable antibody–GNR conjugates that enable an optimized conjugation protocol can overcome several limitations of citrate stabilized gold nanomaterials.

C-reactive protein (CRP) was used as a model target to demonstrate the proof-of-concept. A pair of antibodies capable of specifically recognizing C-reactive protein was used to prepare the LFA. Different protocols for functionalization of GNR were studied regarding the sensitivity for LFA. Two GNR with different colours were used to show the promising properties of GNR based LFA. GNR enables expanding the multiplexing capability of the technique, while retaining most advantages of traditional visual LFA, such as equipment-free detection (by using coloured probes), simplicity of result decoding also by untrained end-users (one colour/one target), cost-effectiveness (based on well-established protocols and cheap materials), and sensitivity.

## 2. Material and methods

### 2.1. Proteins and reagents

Phosphate buffered saline (10xPBS: 1.2 M NaCl, 0.24 M Na2HPO4, 0.06 M NaH2PO4, pH 7.3), MES buffered solution (0.1 M, pH 5.5) and sodium chloride solutions were prepared from the corresponding salts obtained from Roth.

Gold(III) chloride solution ($HAuCl_4$), sodium borohydride ($NaBH_4$) and Cetrimonium bromide (CTAB), N-(3-Dimethylaminopropyl)-N′-ethylcarbodiimide (EDC), N-Hydroxysulfosuccinimide sodium salt (s-NHS) and carboxyl and thiol cross-linking reagents like Poly(ethylene glycol) 2-mercaptoethyl ether acetic acid (HS-PEG1000-COOH and HS-PEG2100-COOH), 16-Mercaptohexadecanoic acid (MHDA) and 3-Mercaptopropionic acid (MPA) were obtained from Sigma–Aldrich.

The monoclonal antibodies (mAb) anti-human CRP 251-226 (anti-h CRP capture mAb) and anti-human CRP 251-227 (anti-h CRP detection mAb) (both monoclonal, IgG) were received from Senova (Weimar, Germany). The human C-reactive protein (CRP) antigen was obtained from BioTrend (Cologne, Germany). Casein buffer (5.5%) were obtained from SDT (Baseweiler, Germany). Bovine serum albumin (BSA) was received from Serva.

Sartorius Unisart CN140, Ahlstrom Grade 222 as absorbent cellulose

pad and glass microfiber Filter Paper (Ahlstrom Grade 161) was used as conjugate and sample pad. Water was obtained from a Millipore® unit. All other chemicals were purchased from standard commercial sources at analytical grade.

### 2.2. Gold nanorods synthesis

GNR were prepared by a method according to Liopo (Liopo et al., 2012). The basic procedure is tailored to the tuning of LSPR peaks <700 nm. In a typical procedure Au Seeds were prepared by adding 5 mL of an 0.5 mM $HAuCl_4$ solution to 5 mL of a 200 mM CTAB solution followed by 50 μL of an icecold 0.2 M $NaBH_4$ solution at 30 °C. This seed solution was used 2-3 h after its preparation. In the next step, exact proportions of 30 mL of 0.05 M CTAB, 600 μL of 0.5 M sodium salicylate (Na-Salicylate), 3-10 μL of 100 mM silver nitrate ($AgNO_3$) and 850 μL of 0.02 M $HAuCl_4$ solutions were added in the preceding order. After 10 min incubation, 30 μL of the seed solution was added. The solution was stirred over night at 30 °C to obtain coloured GNR.

### 2.3. GNR functionalization

COOH-modified GNR were prepared as follows. A solution of GNR (OD = 4) containing CTAB was centrifuged at 14,000 g for 10 min, decanted, and re-dispersed in 2 mL water to remove excess CTAB. 0.5-250 μL of a 2 mM solution of carboxyl and thiol cross-linking reagents were added to the GNR solution. The mixture was stirred for 24 h at room temperature, and was centrifuged at 14,000 g for 10 min, decanted, and re-dispersed in 2 mL water to remove excess reagents.

### 2.4. GNR antibody conjugation

The anti-h CRP 251-227 mAb was used for conjugation with COOH-functionalized GNR. Before conjugation, the carboxyl group of the GNR was activated following this procedure: 1000 μL of functionalized GNR (OD = 1) was mixed with 50 μL MES buffer (pH 5.5, 100 mM), 5 μL of an EDC solution (5 mg/mL) and 5 μL of an s-NHS solution (5 mg/mL) to react for 30 min at RT. Then the excess EDC and s-NHS was removed by washing through centrifugation at 10,000 RCF and re-dispersed in 1000 μL water. After adding 100 μL of 120 mM PBS solution, 20 μg antibody was added to the activated GNR particles. After 1 h incubation, a blocking step by adding 50 μL of a 10% (w/w) BSA solution was performed, followed by centrifugation for 10 min at 10,000 RCF to remove excess reagents. After discarding the supernatant, the pellets were washed, centrifuged, and re-dispersed in 40 μL of an aqueous solution containing 20 mM PBS, 0.5% BSA, 0.25% Tween 20, and 10% sucrose (500 μg antibody/mL).

### 2.5. Synthesis and conjugation of spherical gold nanoparticles

Spherical gold nanoparticles (GNP) were synthesized by the seeded-growth method as described in (Bastús et al., 2011). First, 0.5 mL of 25 mM HAuCl4 solution was added to 75 mL of 2.2 mM sodium citrate solution and brought to a boil. The resulting gold seed solution was cooled to 90 °C. To this solution, 0.5 mL of 60 mM sodium citrate and 0.5 mL of 25 mM HAuCl4 solution were sequentially added 8 times at 2 min intervals to ensure complete mixing after each addition. The mixture was boiled for 25 min, cooled, and stored at 4-6 °C. 10 μg anti-h CRP 251-227 were added to a 1000 μL GNP solution (OD = 1; pH 7.0). After 1 h incubation, a blocking step by adding 50 μL of a 10% (w/w) BSA solution was performed, followed by centrifugation for 10 min at 10,000 RCF to remove excess reagents. After discarding the supernatant, the pellets were washed, centrifuged, and re-dispersed in 40 μL of an aqueous solution containing 20 mM PBS, 0.5% BSA, 0.25% Tween 20, and 10% sucrose (500 μg antibody/mL).

### 2.6. Preparation of lateral flow assay strips

For preparing the test strips, comprised of a sample pad, a conjugate pad, nitrocellulose membrane, and an absorbent pad, a specific capture mAb anti-h CRP 151-226 was immobilized at the test zone. After the membrane and the absorbent pad were attached onto the backing card, capture antibody solution (anti-CRP 151-226, 500 μg/mL) and goat anti-mouse IgG antibody solution (500 μg/mL) in PB buffer (0.1 M, pH 7.3) were dispensed in different zones (test line and control line) on the nitrocellulose membrane by a dispenser system (BioDot XYZ-3000 dispensing platform, 1 μL antibody solution/cm). Subsequently, the dispensed membrane was dried at 37 °C for 2 h.

The gold nanomaterial antibody conjugates were diluted to an antibody concentrations of 250 μg antibody/mL in a PB buffer (0.03 mol/L, pH 7.3, 1% BSA, 1% sucrose) and these suspensions were dispensed (10 μL/cm) in a glass fiber membrane with a BioDot XYZ-3000 dispensing platform to obtain antibody loaded conjugate pads. The conjugate pads were dried for 2 h at 37 °C. The loaded conjugate pad and the sample pad (untreated glass fiber membrane) were then also attached onto the backing card and cut into test stripes (4 × 60 mm) by means of a CM4000 guillotine (Biodot, Irvine, CA). The test strips were mounted into lateral flow housings (Senova, Weimar, Germany) and are ready for use.

### 2.7. GNR characterization

UV–Vis spectra of gold nanomaterial samples were recorded on a Thermo Multiskan GO UV/Vis Microplate Spectrophotometer multi Plate reader in the range of 400–1000 nm with a resolution of 1 nm. The size and morphologies of the obtained gold nanomaterial were characterized by transmission electron microscopy (TEM) (JEOL, JEM-1400). For zeta potential, samples were analyzed using a Zetasizer Nano ZS (Malvern Instruments). All of these samples were analyzed three times at 25 °C with an equilibrium time of 300 s.

### 2.8. Lateral flow assay measurements

CRP solution of various concentrations were prepared in a PBS buffer with 1% Casein. A volume of 100 μL of the CRP solutions was added to the sample pad of a test strip. After 10 min the strips were scanned with a lateral flow reader (opTrilyzer®Med Lateral Flow Reader).

## 3. Results and discussion

### 3.1. Preparation and characteristics of GNR with LSPR less than 700 nm

Seed-mediated growth in the presence of the cationic surfactant CTAB has been continuously improved since its first demonstration by Jana and is now widely adopted for the preparation of GNR (Jana et al., 2001). GNR obtained typically exhibit LSPR greater than 700 nm and a weaker transverse plasmon peak, visible at around 525 nm, and therefore have a red colour. Ye describes an improved size tunable GNR synthesis using aromatic additives. This method allows a reproducible synthesis of GNR with a longitudinal surface plasmon resonance in a visible range. To obtain GNR with a LSPR shorter than 700 nm we use the method according to Ye (Ye et al., 2012). Na-Salicylat was used as additive and the synthesis was optimized by varying the amount of silver nitrate in the seeded growth solution to fine tune the peak of the LSPR band.

GNR produced as described were characterized by UV-Vis spectrometry (Fig. 1a) and TEM imaging (Fig. 1c). The UV-Vis spectra showed strong SPR bands, with $\lambda_{max}$ at 525 nm and a tunable band between 635 – 677 nm (Fig. 1b) to obtain violet and blue GNR. The TEM images show that the length of the particle is around 50 nm and the shape of the nanomaterial changed from square shaped to rod-like shaped. That could be expected since different publications describe a

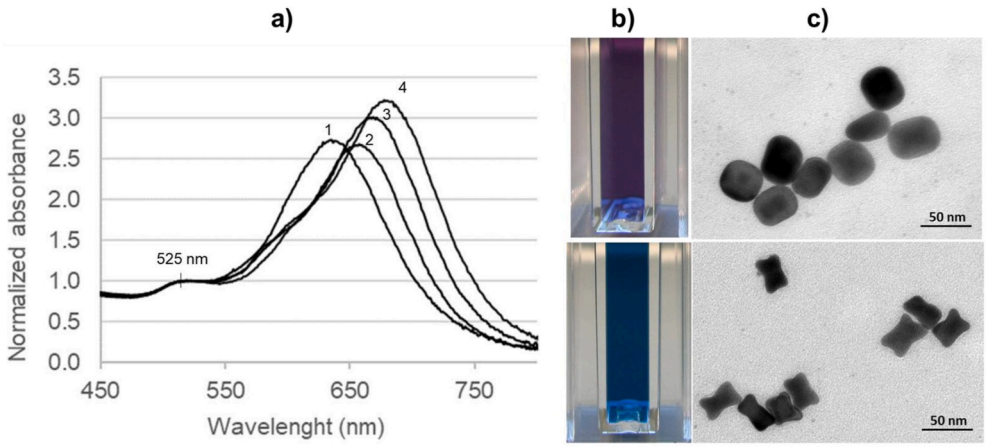


**Fig. 1.** Multicoloured GNR obtained by using different silver contents (1-4). a) spectra of GNR with different LSPR peaks ($\lambda_{max}$ = 635 nm (1), 657 nm (2), 666 nm (3) and 677 nm (4). b) Cuvettes with violet (1) and blue GNR (4). c) TEM images of violet (1) and blue (4) GNR. (For interpretation of the references to colour in this figure legend, the reader is referred to the Web version of this article.)

red shift of the LSPR peak with increasing length/width ratio of nanorods. Furthermore, the increase in rod shape with deviating red shift of the absorption maximum is in accordance to the literature (Scarabelli et al., 2015; Wang and Tang, 2015).

### 3.2. *Surface modification of GNR by chemisorption of carboxyl and thiol cross-linking reagents*

Antibody conjugated rods were prepared by functionalizing the blue GNR (4) with carboxyl and thiol cross-linking reagents in a first step and a conjugation procedure using the EDC/s-NHS chemistry in a second step.

Carboxyl and thiol cross-linking reagents are widely used as functionalization agents for gold nanoparticles. The design of these reagents is primarily focused on the affinity of the thiol group to the gold nanoparticle surface. Moreover, the design permits facile derivatization of these nanomaterials with biomolecules via the vacant carboxyl group. The spacer between these two groups can be modified to meet the application specified requirements like hydrophobia/hydrophobic balance, PEG spacer for preventing unspecific binding events, charge density of the surface (Shenoy et al., 2006; Tsai et al., 2010; Lin et al., 2017).

The COOH functionalization is reached by mixing the carboxyl and thiol cross-linking reagent with GNR stabilized by CTAB (CTAB-GNR). After anchoring of the cross-linking reagent to the GNR surface, CTAB was removed by centrifugation, decantation and re-dispergation in water. The method of bifunctional linkage is easier, faster, and more efficient, in comparison with other methods that remove CTAB and along with optimizing the spacer can be successfully used for long-time storage.

The functionality of antibodies modified on nanomaterials mainly depends on the spacer of the linker and also the surface properties, for example the density of COOH groups (Manson et al., 2011). In this study, four different reagents a) 3-Mercaptopropionic acid (MPA), b) 16-Mercaptohexadecanoic (MHDA) acid and two different PEGylated thiol reagents c) COOH-PEG1000-SH (Mw = 1 kDa) and d) COOH-PEG2100-SH (Mw = 2.1 kDa) and different concentrations of these reagents in the functionalization step were used to modify the blue GNR.

To confirm the chemical modification by functionalization of the GNR, we investigated the zeta potential (Table 1). The zeta potential of the CTAB-GNR complex was highly positive due to the presence of the positively charged CTAB molecules. After functionalization, a negative zeta potential confirmed the chemical change of GNR surfaces: the CTAB bi-layer was removed and the reagent has bound to the surface. Using MPA, the reagent with a very short spacer, the colour of the functionalized GNR changed during the functionalization from blue to slightly grey indicating the aggregation of the GNR. No stabilizing functionalization could be reached. The functionalization by using the reagents MHDA and COOH-PEG-SH spacers leads to stable carboxyl modified GNR, depending on the reagent concentration. Aggregation was observed for all reagents, when the reagent concentration was too low to stabilize GNR. This is in accordance to the results of Wang, who also find out that a minimum amount of thiol reagents is necessary to stabilize gold nanoparticles (Wang et al., 2013). The minimum concentration of the functional reagents differs from reagent to reagent. A concentration of 5 μM MHDA was necessary to achieve stable, functionalized GNR, while for both PEG reagents, 2 μM are enough for stabilization. This suggests that the PEG spacers stabilize the nanomaterials better than the short-chain alkane spacer. Higher reagent concentrations lead not to an increased zeta potential, indicating that the minimum amount has the same stabilizing affect as higher concentrations. No difference in the zeta potential was observed using three different spacers, indicating that similar numbers of carboxyl groups are introduced on the GNR surface. Zeta potential changes confirm chemical modifications on the surface, and correspond to previously published data (Liopo et al., 2012; Wang

**Table 1**
Zeta-Potential (mV) for CTAB coated GNR stock solution (CTAB) and COOH modified GNR after modification with different reagents and different reagent concentrations.

| Surface modification | Carboxyl and thiol cross-linking reagent concentration | | | | |
|---|---|---|---|---|---|
| | 0.5 μM | 2 μM | 10 μM | 50 μM | 250 μM |
| CTAB | | | +35 mV | | |
| MPA | aggregated | aggregated | aggregated | aggregated | aggregated |
| MHDA | aggregated | aggregated | -17 mV | -20 mV | -15 mV |
| COOH-PEG1000-SH | aggregated | -13 mV | -17 mV | -18 mV | -14 mV |
| COOH-PEG2100-SH | aggregated | -12 mV | -16 mV | -14 mV | -18 mV |

et al., 2013).

### 3.3. Stability study

Typical citrate-stabilized nanomaterials are extremely sensitive to environmental influences such as salt concentrations or contamination. Gold nanoparticles aggregate quickly when small amounts of salts are added, or when they get in contact with certain surfaces or contaminants. For example, introducing citrate-based gold conjugates into porous membranes or improperly stored citrate stabilized particles can quickly lead to aggregation (Manson et al., 2011). Increasing the ionic strength induces instability and aggregation of GNP. The modified GNR, however, are stable against such influences. To prove this, a stability test was carried out in which various NaCl concentrations were added to the modified GNR.

As shown in Fig. 2, aggregation of citrate stabilized GNP can be observed by the colour change from red to violet to grey, whereas the modified GNR were still separated also by the highest salt concentrations (no colour change can be observed). It is irrelevant what kind of spacer was attached. All the reagents and cross-linking reagents concentrations used, lead to very stable GNR.

### 3.4. LFA measurements with antibody functionalized GNR by using different functionalization protocols

Once functionalized, the blue GNR (4) are stable in various buffer solutions and also own carboxyl groups, so that antibodies can be coupled covalent via EDC/s-NHS chemistry to the GNR surface. 20 μg antibody per OD and mL was offered during conjugation, to ensure that the GNR were completely modified with antibodies.

In order to enable CRP detection using blue antibody modified GNR, which were functionalized with bifunctional crosslinkers previously, the principle of detection has to be selected. As shown in the schematic (Fig. 3) the components of a lateral flow chromatography assay include a sample pad (SP), conjugate pad (CP), nitrocellulose membrane (NC), and wick/absorbent pad. NC membrane was modified with anti h CRP 251-227 antibody for the test line and anti-mouse IgG antibody for the control line. The different modified GNR were dispensed on the conjugate pad.

For developing an optical signal depending on the CRP concentration, the sample solution was added to the sample pad and the tests were incubated for 10 min. During the assay, mAb-GNR conjugates were released from the conjugate pad. The CRP in the sample and the mAb-GNR build a complex and migrate along the membrane. When reaching the test zone, the complexes were captured by the antibodies on the test zone resulting in the accumulation of GNR conjugates at the test zone. A blue band was observed, and the colour intensity of the test line was directly proportional to the amount of analyte (CRP) in the sample solution. The solution continued to flow until it passed through the control zone where the excess GNR conjugates were captured by the secondary antibody (anti-mouse IgG) to produce a band as positive control. The intensity of the test line was quantified by a LFA reader.

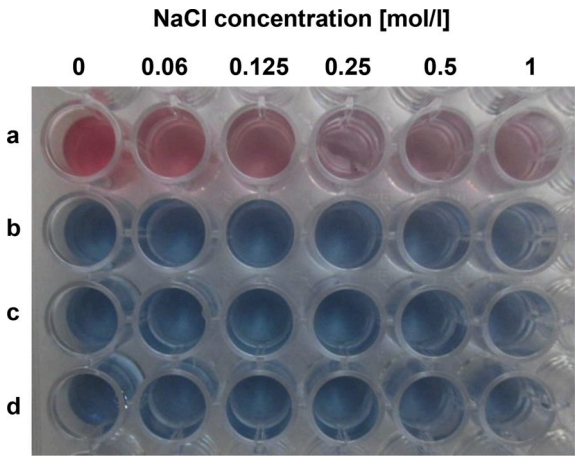


**Fig. 2.** Surface plasmon resonance (SPR) of different gold nanomaterials with different sodium chloride concentrations: a) Citrate stabilized gold nanoparticles, b) GNR functionalized with MHDA, c) GNR functionalized with COOH-PEG1000-SH and d) GNR functionalized with COOH-PEG2100-SH. (For interpretation of the references to colour in this figure legend, the reader is referred to the Web version of this article.)

To optimize the specific optical signal six CRP concentrations ($c_{CRP}$ = 0.5, 2.5, 10, 50, 250 ng/mL) were applied for nine different lateral flow assays, treated with different antibody conjugated GNR, which were prepared with different carboxyl and thiol cross-linking reagents and different concentrations of these reagents.

As shown in Fig. 4, the use of the COOH-PEG-SH reagents as cross-linking reagent, results in lower assay sensitivity. Better results were achieved by using the reagent with a shorter spacer between the SH and COOH group (MHDA reagent). This indicates that conjugates with shorter spacers lead to better antigen affinity. Using even shorter spacer molecules (for example with only three C-atoms) results in aggregation of the GNR during the functionalization process, which indicates that MPA cannot avoid interactions among each GNR.

Apparently, the spacer length or the PEG spacers have a negative influence on the immobilized antibody functionality. A possible reason could be the interaction of the preferred binding sites on the surface of the antibody with PEG. Or the long PEG chains could sterically prevent the antigen from approaching to the antibody. This would also explain that with a higher PEG coating concentration and a longer PEG spacer the sensitivity in the LFA decreases.

Different reagent concentrations during the functionalization protocol lead also to different optical signals in the LFA. The comparison of the intensities of the test line confirms, that a low concentration of the carboxyl and thiol cross-linking reagent is more suited than using higher carboxyl and thiol cross-linking reagent concentrations independent from the reagent. Higher functionalization reagent concentrations do not lead to an increased carboxyl concentration on the surface. This was shown by the zeta potential results. But the reagent concentration does affect the LFA assay performance. This indicates, that a higher reagent concentration does interact with the particle surface. An increased reagent concentration on the particle surface may lead to the fact that the carboxyl groups are hidden in the spacer shell. This would mean, more spacer molecules on the surface are presented, which would explain that a higher reagent concentration leads to a lower antigen affinity of the conjugates. This also could explain a decrease the absolute potential with increased reagent concentration.

Summarizing, the spacer length in combination with the concentration of the cross-linking reagent influences the functionality of the antibody conjugate. This means the dynamic range of the LFA can be controlled by the functionalization protocol. With regard to the sensitivity of the CRP assay, the results show that the shortest spacer and the lowest reagent amount, which leads to a stable particle, are the method of choice for preparing a highly sensitive lateral flow assay.

### 3.5. Analytical performance

The system was optimized regarding the amount of capture mAb and the amount of detection mAb. Also, the running buffer's composition is one of the main factors in developing a biosensor because it has a significant impact on the efficiency of antibody-antigen binding and the elimination of nonspecific adsorption. Several buffers were tested. The results of the optimization are shown in the supplementary section. The highest Signal-Noise Ratio was obtained with 0.5 μg capture mAb per test, 1.0 μg detection mAb per test and 1% Casein in PBS as a running buffer.

Finally, the optimized system was used for establishing two

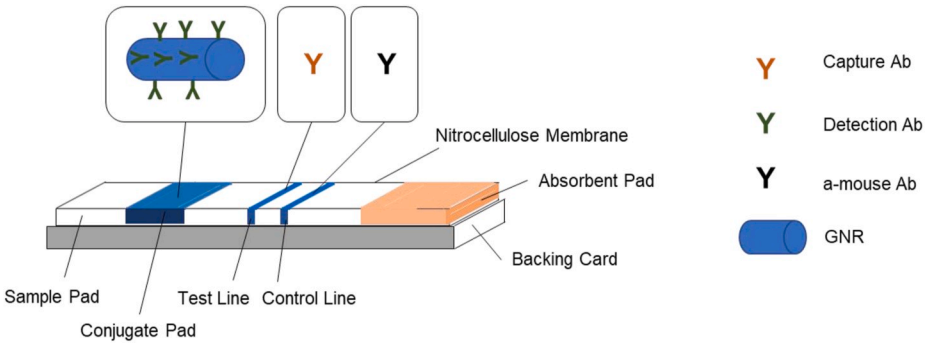


**Fig. 3.** Schematic representation for the configuration of the lateral-flow strip biosensor with the reagents on the different membranes.

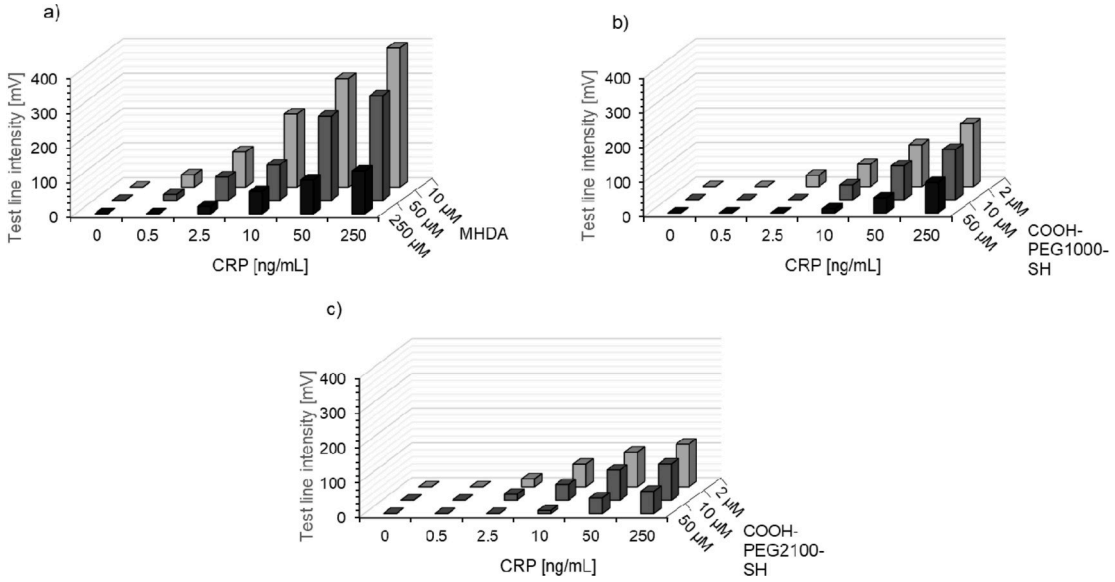


**Fig. 4.** Comparison of the performance of different GNR antibody conjugates in the detection of CRP using an LFA: a) GNR conjugates prepared after functionalization with MHDA, b) GNR conjugates prepared after functionalization with COOH-PEG1000-SH and c) GNR conjugates prepared after functionalization with COOH-PEG2100-SH.

calibration curves for CRP antigen in PBS buffer (1% Casein, pH 7.3) using 1 µg detection antibody per test and 2 µg capture antibody per test. We used the optimized protocols to prepare LFAs with blue GNR (4) and violet GNR (1) as detection reagent. The calibration data is shown in Fig. 5. The limit of detection (LOD) is defined as the summation of the concentration of CRP, corresponding to the mean optical signal of the

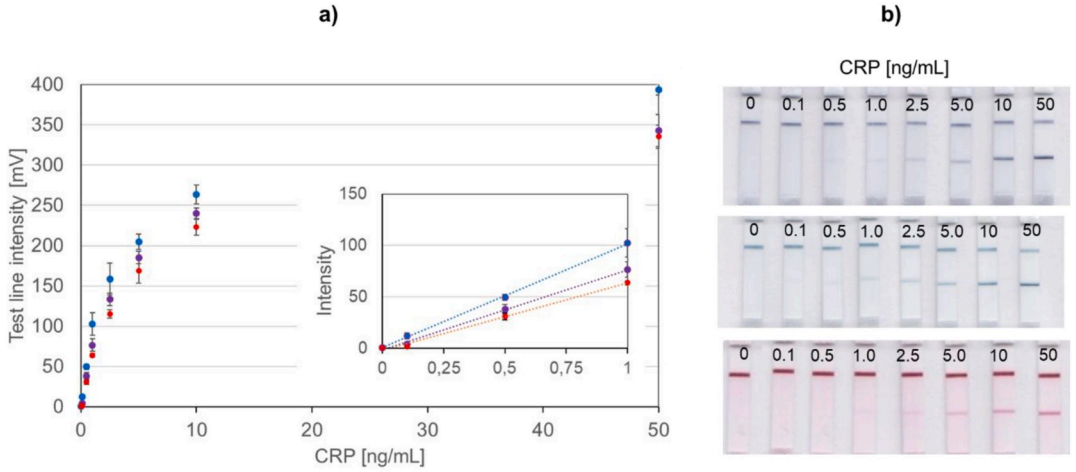


**Fig. 5.** a) Calibration data of the three LFA (using violet GNR (1), blue GNR (4) and GNP (60 nm)). The inset shows the linear response for CRP. Each data point represents the average value obtained from three different measurements. B) Photo images for the three LFA with an increasing CRP concentration (0.1 to 50 ng/mL). (For interpretation of the references to colour in this figure legend, the reader is referred to the Web version of this article.)

zero-dose response, and the threefold standard deviation of this measurement. Using this definition, the LOD was found to be 0.38 ng CRP/mL for the violet GNR conjugates, 0.26 ng CRP/mL for the blue GNR conjugates. Compared to an LFA based on 60 nm colloidal Gold nanoparticles, where the antibodies were attached passively, the sensitivity is 1.9-fold higher (LOD = 0.50 ng CRP/mL).

The blue GNR show a lower detection limit than the violet GNR. This could indicate that a stick shape of the nanomaterial is beneficial for assay sensitivity. Near showed that with increasing shift of the absorption maximum to long wavelengths, the extinction coefficient of the nanomaterials increases (Near et al., 2013). This could explain that better sensitivities are achieved with the blue GNR. In addition, this would mean that a further red shift would be advantageous. However, nanomaterials with optical properties in the near infrared area (>700 nm) would be unsuited for visual read out.

The reproducibility of the blue GNR (4) -based LFA was studied by testing the sample solutions at different concentration levels (0.5, 2 and 10 ng/mL). Samples from the same batch preparation and at the same concentration level were tested 12 times. Similar responses were obtained at the same concentration level. The resulting coefficient of variations (CV)s were 9.1% for low CRP concentrations, 7.5% for medium CRP concentrations and 8.0% for high CRP concentrations. The overall CV for the whole assay was 8.2%, which is quite good for immuno-based detection systems. This also proves the generation of reproducible results using GNR as detection label in LFA application.

This shows that GNR are also promising labels for the visual evaluation of LFA, but the performance depends strongly on the functionalization strategies. Compared to other labels, the detection limit of GNR-based LFA is comparable with LFA using Quantum Dot as label. Nearly the same LOD (0,3 and 0,46 ng/mL) was achieved with quantum Dot based LFA (Lv et al., 2017; Wu et al., 2018) and almost 4-fold lower than an immunomagnetic beads-label assay (Guo et al., 2018).

## 4. Conclusions

Lateral flow assays are among the most commonly used point of care tests and are therefore in the focus of many research groups. Optimizing the sensitivity of the LFA always plays a major role. The most common labels include gold nanoparticles with passively bound antibodies. In this study, a new type of nanogold label was considered to improve the sensitivity of LFA. To our knowledge the first time visual GNR with covalently bound antibodies were applied as a label in LFA. It was shown, that the sensitivity of the LFA can be optimized by varying the type of cross-linking reagent and their used concentration during the functionalization step. Furthermore, the morphology of the GNR also affects the sensitivity of the LFA. Using thinner GNR compared to thicker GNR nanomaterial (with similar length), the sensitivity can be increased 1.5 times.

In this work the LFA based CRP detection using optimized GNR is highly sensitive (detection limit 0.26 ng CRP/mL). Furthermore, the protocols give the advantage of preparing different coloured GNR for improved multiplexing. The highly sensitive CRP detection indicates the possibilities of using GNR as visual label and we also show how to optimize the antibody conjugates by different functionalization protocols.

## Declaration of competing interest

The authors declare that they have no known competing financial interests or personal relationships that could have appeared to influence the work reported in this paper.

## CRediT authorship contribution statement

**Friedrich Scholz:** Conceptualization, Methodology, Formal analysis, Investigation, Resources, Writing - original draft, Visualization, Project administration, Funding acquisition. **Theresa Heckmann:** Investigation. **Lisa Freund:** Investigation. **Anne-Marie Gad:** Resources, Investigation, Writing - review & editing. **Tobias Fischer:** Investigation. **Andreas Gütter:** Resources, Funding acquisition. **Hans Hermann Söffing:** Resources, Writing - review & editing, Supervision.

## Acknowledgments

We acknowledge the Leibniz Institute of Age Research – Fritz Lipmann Institute (FLI) Jena providing access to TEM and Katrin Buder (FLI) for help with TEM.

This work was financially supported by the Federal Ministry for Economic Affairs and Energy (BMWi) (Project No.: ZF4009905MD9).

## Appendix A. Supplementary data

Supplementary data to this article can be found online at https://doi.org/10.1016/j.bios.2020.112324.

## References

Anfossi, L., Di Nardo, F., Russo, A., Cavalera, S., Giovannoli, C., Spano, G., Baumgartner, S., Lauter, K., Baggiani, C., 2019. Anal. Bioanal. Chem. 411, 1905–1913.
António, M., Nogueira, J., Vitorino, R., Daniel-da-Silva, A.L., 2018. Nanomaterials 8 (4), 200.
Aveyard, J., Mehrabi, M., Cossins, A., Braven, H., Wilson, R., 2007. Chem. Commun. 41, 4251–4253.
Bastús, N.G., Comenge, J., Puntes, V., 2011. Langmuir 27, 11098–11105.
Di Nardo, F., Baggiani, C., Giovannoli, C., Spano, G., Anfossi, L., 2017. Microchim. Acta. 184, 1295–1304.
Di Nardo, F., Alladio, E., Baggiani, C., Cavalera, S., Giovannoli, C., Spano, G., Anfossi, L., 2019. Talanta 192, 288–294.
Dreaden, E.C., Alkilany, A.M., Huang, X., Murphy, C.J., El-Sayed, M.A., 2012. Chem. Soc. Rev. 41, 2740–2779.
Dzantiev, B., Byzova, N.A., Urusov, A.E., Zherdev, A.V., 2014. Trends Anal. Chem. 55, 81–93.
Fu, X., Cheng, Z., Yu, J., Choo, P., Chen, L., Choo, J., 2016. Biosens. Bioelectron. 78, 530–537.
Gao, J., Huang, X., Liu, H., Zan, F., Ren, J., 2012. Langmuir 28, 4464–4471.
Guler, Z., Sarac, A., 2016. Express Polym. Lett. 10, 96–110.
Guo, L., Yang, Z., Zhi, S., Feng, Z., Lei, C., Zhou, Y., 2018. PloS One 13 (3), e0194631.
Henderson, K., Stewart, J., 2002. J. Immunol. Methods 270, 77–84.
Huang, X., Aguilar, Z.P., Xu, H., Lai, W., Xiong, Y., 2016. Biosens. Bioelectron. 75, 166–180.
Huff, T.B., Hansen, M.N., Zhao, Y., Cheng, J.X., Wei, A., 2007. Langmuir 23, 1596–1599.
Jana, N.R., Gearheart, L., Murphy, C.J., 2001. J. Phys. Chem. B 105, 4065–4067.
Ji, Y., Ren, M., Li, Y., Huang, Z., Shu, M., Yang, H., Xiong, Y., Xu, Y., 2015. Talanta 142, 206–212.
Kavosi, B., Hallaj, R., Teymourian, H., Salimi, A., 2014. Biosens. Bioelectron. 59, 389–396.
Koczula, K.M., Gallotta, A., 2016. Essays Biochem. 60, 111–120.
Laitinen, M.P.A., Vuento, M., 1996. Biosens. Bioelectron. 11, 1207–1214.
Lee, B., Park, J.H., Byun, J.Y., Kim, J.H., Kim, M.G., 2017. Biosens. Bioelectron. 102, 504–509.
Liao, H., Hafner, J., 2005. Chem. Mater. 17, 4636–4641.
Lin, L.K., Uzunoglu, A., Stanciu, L.A., 2017. Small 14 (10), 1702828.
Lin, L.K., Huang, P.Y., Dutta, S., Rochet, J.C., Stanciu, L.A., 2019. Part. Part. Syst. Char. 36, 1900133.
Liopo, A., Conjusteau, A., Tsyboulski, D., Ermolinsky, B., Kazansky, A., Oraevsky, A., 2012. J. Nanomed. Nanotechnol. 2 https://doi.org/10.4172/2157-7439.S2-001.
Liu, X., Jinhai, A., Huo, Q., 2007. Colloids Surf. B Biointerfaces 58, 3–7.
Lu, L., Yu, J., Liu, X., Yang, X., Zhou, Z., Jin, Q., Xiao, R., Wang, C., 2020. RSC Adv. 10 (1), 271–281.
Lv, Y., Wu, R., Feng, K., Li, J., Mao, Q., Yuan, H., Shen, H., Chai, X., Li, L.S., 2017. J. Nanobiotechnol. 15 (1), 35–44.
Maiorano, G., Rizzello, L., Malvindi, M.A., Shankar, S.S., Martiradonna, L., Falqui, A., 2011. Nanoscale 3, 2227–2232.
Manson, J., Kumar, D., Meenan, B.J., Dixon, D., 2011. Gold Bull. 44, 99–105.
Meissner, J., Prause, A., Bharti, B., Findenegg, G.H., 2015. Colloid Polym. Sci. 293, 3381–3391.
Near, R.D., Hayden, S.C., Hunter, R.E., Thackston, D., El-Sayed, M.A., 2013. J. Phys. Chem. C 117, 23950–23955.
Nguyen, V.T., Song, S., Park, S., Joo, C., 2020. Biosens. Bioelectron. https://doi.org/10.1016/j.bios.2020.112015.
Parolo, C., de la Escosura-Muñiz, A., Merkoç, A., 2013. Biosens. Bioelectron. 40, 412–416.
Petrakova, A.V., Urusov, A.E., Zherdev, A.V., Dzantiev, B.B., 2019. Anal. Biochem. 568, 7–13.

Posthuma-Trumpie, G.A., Korf, J., van Amerongen, A., 2009. Anal. Bioanal. Chem. 393, 569–582.
Puertas, S., Batalla, P., Moros, M., Polo, E., del Pino, P., Guisán, J.M., Grazú, V., de la Fuente, J.M., 2011. ACS Nano 5, 4521–4528.
Sajid, M., Kawde, A.N., Daud, M., 2015. J. Saudi Chem. Soc. 19, 689–705.
Scarabelli, L., Sánchez-Iglesias, A., Pérez-Juste, J., Liz-Marzán, L.M., 2015. J. Phys. Chem. Lett. 6, 4270–4279.
Serebrennikova, K., Samsonova, J., Osipov, A., 2018. Nano-Micro Lett. 10, 24–31.
Shenoy, D., Fu, W., Li, J., Crasto, C., Jones, G., DiMarzio, C., Sridhar, S., Amiji, M., 2006. Int. J. Nanomed. 1 (1), 51–57.
Shin, J.H., Park, J.K., 2016. Anal. Chem. 88, 10374–10378.
Tsai, D.H., DelRio, F.W., MacCuspie, R.I., Cho, T.J., Zachariah, M.R., Hackley, V.A., 2010. Langmuir 26 (12), 10325–10333.
Tao, Y., Yang, J., Chen, L., Huang, Y., Qiu, B., Guo, L., Lin, Z., 2018. Microchimica Acta 185 (7). Article Number: UNSP 350 Published: JUL 2018.
Tshikhudo, T.R., Wang, Z., Brust, M., 2004. Mater. Sci. Technol. 20, 980–984.
Venkataramasubramani, M., Tang, L., 2009. 25th Southern Biomedical engineering conference. IFMBE Proc. 24, 199–202.
Wang, W., Wie, Q.Q., Wang, J., Wang, B.C., Zhang, S.H., Yuan, Z., 2013. J. Colloid Interface Sci. 404, 223–229.
Wang, Y., Tang, L., 2015. Biosens. Bioelectron. 67, 18–24.
Wang, X., Mei, Z., Wang, Y., Tang, L., 2017. Beilstein J. Nanotechnol. 8, 372–380.
Wiriyachaiporn, N., Maneeprakorn, W., Apiwat, C., Dharakul, T., 2015. Microchim. Acta. 182, 85–93.
Wu, R., Zhou, S., Chen, T., Li, J., Shen, H., Chai, Y., Li, L.S., 2018. Anal. Chim. Acta 1008, 1–7.
Xie, Q.Y., Wu, Y.H., Xiong, Q.R., Xu, H.Y., Xiong, Y.H., Liu, K., Jin, Y., La, W.H., 2014. Biosens. Bioelectron. 54, 262–265.
Ye, X., Jin, L., Caglayan, H., Chen, J., Xing, G., Zheng, C., Doan-Nguyen, V., Kang, Y., Engheta, N., Kagan, C.R., Murray, C.B., 2012. ACS Nano 6 (3), 2804–2817.
Zhang, L., Huang, Y., Wang, J., Rong, Y., Lai, W., Zhang, J., Chen, T., 2015. Langmuir 31, 5537–5554.
Zhu, M., Zhang, J., Cao, J., Ma, J., Li, X., Shi, F., 2019. Anal. Bioanal. Chem. 411 (30), 8033–8042.